Available online at www.sciencedirect.com

SCIENCE DIRECT

Biochimica et Biophysica Acta 1706 (2005) 220–231

BIOCHIMICA ET BIOPHYSICA ACTA BBA

http://www.elsevier.com/locate/bba

Sequential assembly of photosynthetic units in *Rhodobacter sphaeroides* as revealed by fast repetition rate analysis of variable bacteriochlorophyll *a* fluorescence

Michal Koblízek[a,b], Joseph D. Shih[c], Seth I. Breitbart[c], Emma C. Ratcliffe[d], Zbigniew S. Kolber[a,e], C. Neil Hunter[d], Robert A. Niederman[c,*]

[a]*Environmental Biophysics and Molecular Ecology Program, Rutgers University, 71 Dudley Road, Institute of Coastal and Marine Sciences, New Brunswick, NJ 08901-8521, USA*

[b]*Institute of Microbiology and Institute of Physical Biology, Opatovicky mlyn, 379 81 Trebon, Czech Republic*

[c]*Department of Molecular Biology and Biochemistry, Rutgers University, 604 Allison Road, Nelson Biological Laboratories, Piscataway, NJ 08854-8082, USA*

[d]*Department of Molecular Biology and Biotechnology, University of Sheffield, Sheffield S10 2TN, UK*

[e]*Monterey Bay Aquarium Research Institute, 7700 Sandholdt Road, Moss Landing, CA 95039, USA*

Received 1 March 2004; received in revised form 27 October 2004; accepted 10 November 2004
Available online 28 November 2004

Abstract

The development of functional photosynthetic units in *Rhodobacter sphaeroides* was followed by near infra-red fast repetition rate (IRFRR) fluorescence measurements that were correlated to absorption spectroscopy, electron microscopy and pigment analyses. To induce the formation of intracytoplasmic membranes (ICM) (greening), cells grown aerobically both in batch culture and in a carbon-limited chemostat were transferred to semiaerobic conditions. In both aerobic cultures, a low level of photosynthetic complexes was observed, which were composed of the reaction center and the LH1 core antenna. Interestingly, in the batch cultures the reaction centers were essentially inactive in forward electron transfer and exhibited low photochemical yields F_V/F_M, whereas the chemostat culture displayed functional reaction centers with a rather rapid (1–2 ms) electron transfer turnover, as well as a high F_V/F_M of ~0.8. In both cases, the transfer to semiaerobiosis resulted in rapid induction of bacteriochlorophyll *a* synthesis that was reflected by both an increase in the number of LH1–reaction center and peripheral LH2 antenna complexes. These studies establish that photosynthetic units are assembled in a sequential manner, where the appearance of the LH1–reaction center cores is followed by the activation of functional electron transfer, and finally by the accumulation of the LH2 complexes.

Keywords: Membrane development; Light-harvesting complex; Photosynthetic membrane; Fast repetition rate fluorescence; Reaction center kinetics

1. Introduction

Kinetic measurements of chlorophyll fluorescence have become routine in photosynthesis and plant physiology research [1]. In oxygenic phototrophs, chlorophyll fluorescence provides valuable information on the energetics of primary photosynthetic reactions, the extent and nature of photoprotective processes and electron transport rates. Similarly to photosystem II (PSII) in oxygenic phototrophs, variable fluorescence in anoxygenic phototrophic purple bacteria is related to the presence of pheophytin-

Abbreviations: bc_1 complex, ubiquinol-cytochrome c_2 oxidoreductase; BChl *a*, bacteriochlorophyll *a*; CM, cytoplasmic membrane; IRFRR, infra-red fast repetition rate; F_0, minimal fluorescence yield; F_M, maximal fluorescence yield; F_V, variable fluorescence (difference between F_0 and F_M); ICM, intracytoplasmic membrane; LH1, core light-harvesting complex; LH2, peripheral light-harvesting complex; *p*, energy transfer between photosynthetic units; P_{870}, reaction center bacteriochlorophyll *a* dimer; PSII, photosystem II; σ, functional absorption cross-section

* Corresponding author. Tel.: +1 732 445 3985; fax: +1 732 445 4213.
E-mail address: rniederm@rci.rutgers.edu (R.A. Niederman).

0005-2728/$ - see front matter © 2004 Elsevier B.V. All rights reserved.
doi:10.1016/j.bbabio.2004.11.004

quinone type reaction centers. It has been used to characterize the processes of light absorption, charge separation, and electron transport in various photosynthetic bacteria [2–7]. Although bacteriochlorophyll fluorescence has been historically recognized as a valuable tool in the study of bacterial photosynthesis, the number of studies of the variable fluorescence of BChl *a* is, in comparison with Chl *a* fluorescence, rather limited. This is likely to be connected with the numerous Chl *a* fluorescence applications in plant physiology, phycology or marine biology, together with the convenience of kinetic absorption measurements to monitor electron transfer reactions in photosynthetic bacteria, which has limited the need for alternative techniques.

Here, we used a newly designed near-IR fast repetition rate (IRFRR) fluorometer to monitor photosynthetic unit development in the facultative photoheterotroph *Rhodobacter* (*Rba*.) *sphaeroides*, a member of the α-3 subclass of the *Proteobacteria*, which provides an ideal experimental system for membrane biogenesis and assembly studies. When grown under anaerobic conditions in the light, *Rba. sphaeroides* forms a system of intracytoplasmic membranes (ICM) that house photosynthetic units consisting of core structures in which the reactions center is surrounded by the light-harvesting (LH) 1 complex, with the LH2 complex arranged at their peripheries. Under these growth conditions, levels of LH2 relative to LH1–reaction center core complexes are related inversely to light intensity [8]. Although ICM formation is repressed by high oxygen tension under chemoheterotrophic conditions, lowering the oxygen partial pressure results in a gratuitous induction of ICM assembly in the dark (greening) by invagination of the cytoplasmic membrane (CM), together with the synthesis and assembly of light-harvesting and reaction center complexes [9]. These developmental changes are under the control of a global two-component oxygen sensing, signal transduction system [10–13], and additional regulatory components that include overlapping aerobic repressor circuits for the repression of bacteriochlorophyll *a* (BChl *a*), carotenoid and LH2 synthesis [14,15], as well as a photoreceptor that integrates both redox and light signals [16,17].

The ability to isolate putative sites of CM invagination permits membrane development in *Rba. sphaeroides* to be conveniently followed by biochemical and biophysical techniques. These membrane domains are obtained in an upper-pigmented band which sediments more slowly than the ICM-derived chromatophore vesicle fraction during rate-zone centrifugation on sucrose density gradients. Pulse-chase [18–20], membrane fractionation [20] and spectroscopic studies [3,21] have shown that, in addition to containing respiratory CM, the upper pigmented fraction is enriched in nascent LH1–reaction center core complexes, which represent "developing centers" that mature into photosynthetic units after further addition of LH2 [18], which drives vesicularization of the ICM [22–25].

In this paper, we demonstrate the applicability of variable BChl *a* fluorescence transients, generated by IRFRR fluorometry, for readily elucidating functional aspects of the photosynthetic unit assembly process. The basic concept of this analysis is that the initial rapid pulse sequence (150-μs time scale) elicits single charge separation in all the reaction centers [26]. The registered variable fluorescence signal reflects the redox status of the reaction center, where low fluorescence yield indicates an open reaction center (no charge, reaction center is ready to perform photochemistry) and high fluorescence yield indicates a closed reaction center (charged reaction center, transiently non-functional photochemistry). The difference between the minimum fluorescence F_0 and maximum F_M serves as an estimate of the quantum yield of the primary charge separation (estimated from the F_V/F_M ratio). The analysis of the induction kinetics provides information of functional absorption cross-section (σ) of the photosynthetic complexes and connectivity (p). Later in the protocol, slow relaxation kinetics are recorded which are assumed to reflect reopening of the reaction center. Our results from both isolated membrane fractions and low-aeration cell suspensions cultured in batches and in a chemostat further demonstrate that the components of the photosynthetic unit are assembled in a sequential rather than simultaneous manner.

2. Materials and methods

2.1. Growth, ICM induction (greening) and membrane isolation procedures

Induction of ICM formation in batch cultures of *Rba. sphaeroides* NCIB 8253 was performed as described previously [27] on a gyratory shaker in a medium with DL-malate as electron donor [8]. Cells grown chemoheterotrophically at high aeration (350 rpm) were washed and resuspended as concentrated suspensions at low aeration (200 rpm) in the dark, and photosynthetic pigment formation was followed for 22–24 h.

For the induction of ICM formation in steady-state cells cultured in a chemostat, malate at a concentration of 5 mM served as the limiting nutrient and the concentration of casamino acids was halved (0.5 g/L). The chemostat was inoculated from a dense batch culture. Cells were grown in a bleached state aerobically for 2 days by pumping air through the chemostat; low-aeration conditions were then established by lowering the oxygen tension to 3% (balanced with N_2). The culture was sampled over a 30-h period for IRFRR measurements, near-IR absorption spectra, pigment analyses and transmission electron microscopy on thin-cell sections.

For membrane isolation, cells grown photoheterotrophically at high light intensity (850 W m^{-2}) were disrupted in a French pressure cell and cell-free extracts were subjected to rate-zone sedimentation on sucrose density gradients [25]

to obtain upper pigmented and chromatophore fractions. The respective distributions of BChl *a* in the isolated fractions were ~32% and 68%.

2.2. Fast repetition rate fluorometry

The IRFRR instrument is a modified version of the fast repetition rate fluorometer originally designed to characterize oxygenic photoautotrophs [26], modified to measure fluorescence signals at 880 nm as described earlier [7]. The light output of the flashing unit was increased about five times (~3×10^4 W m^{-2} excitation power) to obtain sufficient light intensity for saturating bacterial photosynthetic centers. In addition, the instrument was equipped with an infrared laser diode (795 nm) to specifically excite the LH2 complex of purple non-sulfur photosynthetic bacteria. The fluorescence signal, excited by a sequence of submicrosecond flashes, is detected by a large area (16-mm diameter) avalanche photodiode detector with AC coupling (630-70-72-631, Advanced Photonix, Inc.) and protected by RG830 glass and 880-nm interference filters (Intor, 70 nm half-width). Digitized fluorescence kinetic transients obtained at 880 nm are processed by computer-assisted analysis.

The crucial part of the analysis is a mathematical model, which translates the measured signal into several physiological parameters, such as functional absorption cross-section (σ), quantum yield of primary charge separation (F_V/F_M), and electron transfer turnover of the reaction center as described in detail previously [26]. Briefly, the instrument generates a rapid sequence of 120 subsaturating flashlets (flashlet duration 0.5 μs, spacing 1.2 μs, total duration 144 μs), which gradually close the reaction centers. The reaction center closure results in a rise of the fluorescence intensity from initial F_0 level to maximal level denoted as F_M (see Fig. 1). The F_V/F_M ratio (calculated as $F_V/F_M=[F_M-F_0]/F_M$) is frequently used for estimation of the quantum yield of primary photochemistry. The rate of the fluorescence rise provides information on efficiency of light harvesting by the photosynthetic units. Rapid rise signals large and efficient light harvesting complexes whereas slow rise means small or inefficient antennae. The sigmoidicity of the induction provides information on the extent of excitation transfer among the photosynthetic units ("connectivity"). The fluorescence induction elicited by the flashlets is analyzed by a computer-assisted curve fitting algorithm using formulae:

$$f_t = F_0 + (F_M - F_0) \times C_t \times (1-p)/(1-C_t p) \quad (1)$$

$$\partial C_t/\partial I = \sigma_{RC}(1-C_t)/(1-C_t p) \quad (2)$$

where f_t is a fluorescence yield at time t, F_0 and F_M are the minimal and maximal fluorescence, C_t is the fraction of closed reaction centers, p is the connectivity parameter, σ is the functional absorption cross-section and I is irradiance.

After the induction part of the protocol, the reaction centers are allowed to reopen and the process is recorded by

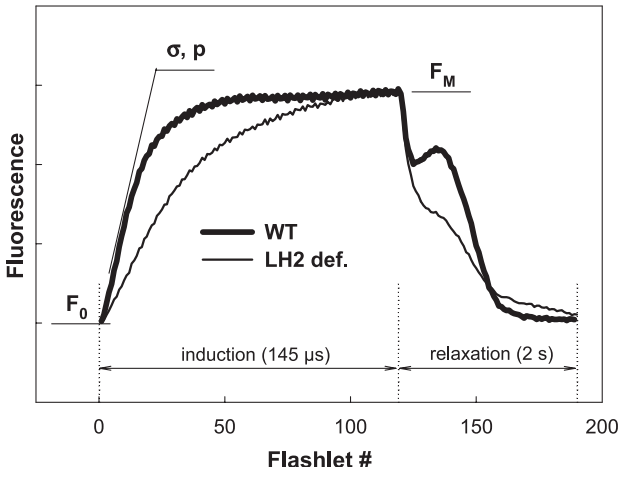

Fig. 1. Fast repetition rate fluorescence kinetic transient elicited upon 470-nm excitation with *Rba. sphaeroides* wild-type (thick line) and LH2-deficient mutant M21 (thin line). The transient has two phases: Phase I-induction, which consists of 120 rapid flashes (0.4-μs duration at 1.2-μs intervals) and results in cumulative closure of the reaction center. For Phase II, 70 flashes are applied at intervals varying exponentially from 20 μs to 50 ms (2.1 s total duration) over which the fluorescence signal is relaxed with kinetics reflecting the reopening of the reaction centers. Parameters: F_0, F_M, minimal and maximal fluorescence yields; p, connectivity; σ, functional absorption cross-section. Note the difference in the rate of fluorescence induction between the wild-type and LH2-deficient mutant, showing the difference in light-harvesting complex cross-section.

70 logarithmically spaced flashlets for 2 s (see Fig. 1). The number and spacing of the flashlets in the relaxation part of the protocol are chosen to minimize their actinic effect. The fluorescence relaxation part of the protocol is deconvoluted into three exponential decay kinetics

$$C_t = 1 - a_1\exp(-t/\tau_1) - a_2\exp(-t/\tau_2) - a_3\exp(-t/\tau_3) \quad (3)$$

where a_x are amplitudes of the individual exponential components, τ_x are time constants and t is time. To parameterize the reaction center relaxation rate by a single parameter, the electron transfer turnover τ_{ET} is calculated as

$$\tau_{ET} = (a_1\tau_1 + a_2\tau_2 + a_3\tau_3)/(a_1 + a_2 + a_3) \quad (4)$$

(note that theoretically $a_1+a_2+a_3=1$ and thus $\tau_{ET}=a_1\tau_1+a_2\tau_2+a_3\tau_3$).

The F_M levels obtained by multiple turnover pulses (tens of milliseconds time scale) were identical to those obtained in single turnover (150 μs) kinetics and are not discussed further. Except for the IRFRR analysis in Fig. 2C, all measurements were made on whole cells diluted typically to about 30 nM BChl *a* to produce transients in the linear range.

2.3. Analytical procedures

Molar ratios of light-harvesting complexes were calculated by deconvoluting near-IR absorption spectra [28] obtained on a Beckman DU-640 spectrophotometer. Pig-

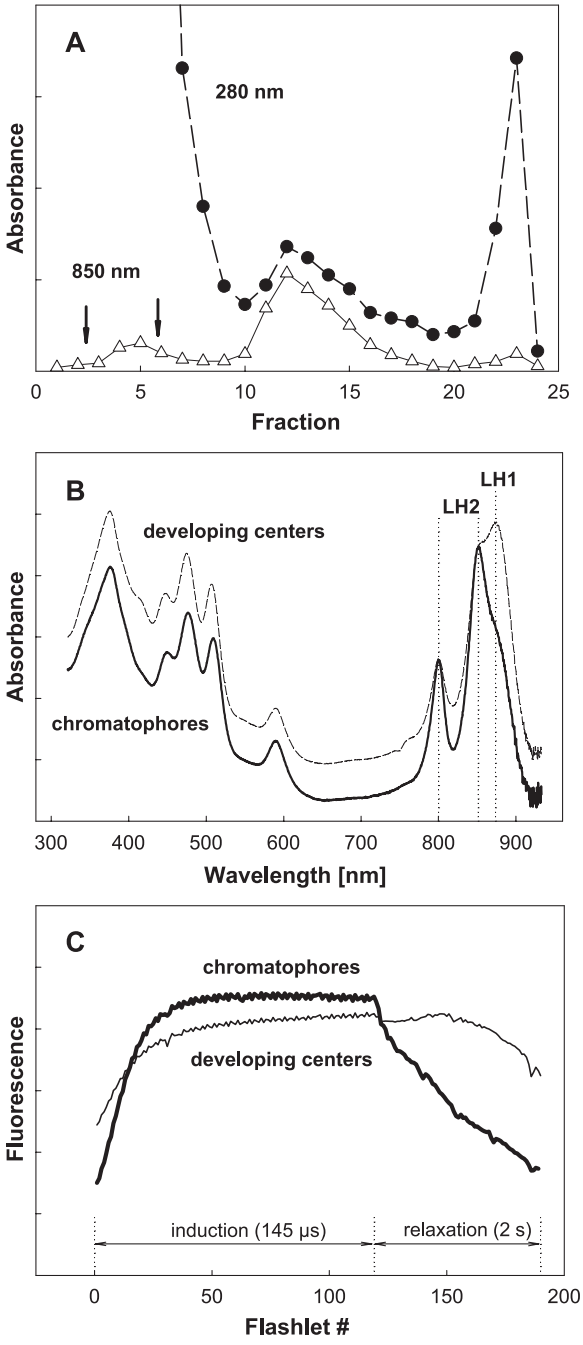

Fig. 2. Analysis of isolated membrane fractions containing photosynthetic units in different developmental stages. (A) Typical rate-zone sedimentation profile of French-pressure cell extract of high light-intensity grown *Rba. sphaeroides* on a 5–35% (w/w) sucrose density gradient [25] showing separation of membranes in different stages of development. Arrows denote upper pigmented band containing the developing centers (banding at 1.04 g ml^{-1}); mature chromatophores are typically collected from fractions 11–15 (banding at 1.09 g ml^{-1}), and essentially unpigmented cell envelope banded in fractions 21–24. BChl *a* was localized from absorbance at 850 nm. Absorbance at 280 nm in top portion of gradient is largely accounted for by ribosomes. (B) Absorption spectra of chromatophores and developing centers in the upper pigmented fraction. In the near-IR, the LH1 complex has an absorption maximum at 875 nm (B875 band) and the LH2 complex has maxima at 800 and 850 nm (B800 and B850 bands). The traces are aligned at 850 nm to highlight LH1 differences. (C) Fluorescence kinetic transient obtained by IRFRR analysis at 880 nm; excitation at 470 nm. Fluorescence is expressed in arbitrary units.

ment composition was analyzed by HPLC [Koblizek et al., submitted for publication] and the levels of spheroidene and spheroidenone were calculated as described previously [27].

2.4. Electron microscopy

Cells were fixed for 3 h in a solution of 1% (v/v) glutaraldehyde and 4% formaldehyde in 0.1 M phosphate buffer, pH 7.3, followed by postfixation for 1 h in 1% OsO_4 prepared in phosphate buffer, dehydration through an ethanol series and embedding in Epon-Araldite. Samples were sectioned with an LKB 2088 ultramicrotome, post-stained with 5% (wt/v) uranyl acetate in 50% ethanol for 15 min, and with 0.5% lead citrate for 2 min. Thin sections were viewed in a JEOL JEM-100 CXII electron microscope.

3. Results

3.1. IRFRR fluorescence measurements with purple non-sulfur photosynthetic bacteria

Fast repetition fluorescence measurements were tested with various strains of anoxygenic phototrophic bacteria, including aerobic species. Typical IRFRR fluorescence transients characteristic of the wild-type and LH2-deficient mutant (M21) of *Rba. sphaeroides* are shown in Fig. 1. Both strains display the same F_V/F_M ratios (Table 1), but they clearly differ in the rate of rapid fluorescence induction, indicative of the different sizes (functional absorption cross-section) of their complement of light harvesting complexes. The M21 mutant lacked an excitable signal at 795 nm (data not shown), since it contains no LH2 complex. On the other hand, $\sigma_{470\ nm}$ values (Table 1) reflect the absorption of both LH1- and LH2-bound carotenoids (the $S_2(1B_u^+)$ state of spheroidene and spheroidenone). Note that LH1 can contribute relatively more to this parameter than it contributes to the total BChl *a* content, since LH1 has a BChl/carotenoid ratio of 1.0, while that for LH2 is near 2.0 [22].

All the species displayed an induction of the variable BChl fluorescence region upon blue (470 nm) excitation. Similar to the M21 mutant, species missing the LH2 complex lacked the 795-nm excitation signal (Table 1). The F_V/F_M ratios determined in all species were consistently high (0.7–0.8), suggesting a high efficiency of primary photochemistry. Photosynthetic bacteria display much lower (3–10 times) functional absorption cross-section values at 470 nm, when compared to those of phytoplankton (not shown). *Rhodospirillum rubrum* gave the smallest $\sigma_{470\ nm}$ value, making it difficult to saturate the variable fluorescence with the excitation power available in the IRFFR instrument. *Rsp. rubrum* also displayed a distinctly sigmoidal fluorescence kinetics, which is usually interpreted in terms of connectivity between photosynthetic units (Table 1).

Table 1
Comparison of the basic variable fluorescence parameters of several strains of photosynthetic bacteria

Organism	F_V/F_M	$\sigma_{470\ nm}$ [Å^2]	$\sigma_{795\ nm}$ [Å^2]	p	LH2
Rhodobacter sphaeroides strain 8253	0.82±0.01	69±2	82±2	0.23±0.04	+
Rhodobacter sphaeroides strain M21	0.77±0.01	28±1	~0	0.23±0.01	−
Rhodobacter capsulatus strain pTB9991[a]	0.81±0.01	106±3	100±2	0.13±0.09	+
Rhodospirillum rubrum S1	0.74±0.01	16±1	~0	0.58±0.02	−
Erythrobacter sp. strain NAP1	0.82±0.02	33±2	~0	0.01±0.01	−
Roseobacter denitrificans	0.74±0.01	42±2	48±5	0.03±0.02	+

All the strains were grown under heterotrophic conditions. *Rba. sphaeroides* mutant M21 does not produce the peripheral light harvesting complex LH2. The parameters were obtained from IRFRR measurements. The standard errors were determined from three repeated measurements using the same batch of cells. Symbol '+' signifies LH2 complex is present, '−' means LH2 is absent.

[a] Kindly supplied by Prof. J.T. Beatty.

3.2. IRFRR fluorescence measurements on isolated membrane fractions

Fig. 2A shows a typical sucrose gradient profile of the isolation of developing centers in the upper pigmented band, and of mature photosynthetic units in the chromatophore fraction, after rate-zone sedimentation. Their absorption spectra (Fig. 2B) indicated that the developing centers contained LH1–reaction center core particles with reduced LH2 levels. After deconvolution of the near-IR region, LH2/LH1 molar ratios of 0.58 and 1.05 were calculated for upper pigmented and chromatophore fractions, respectively. These correspond to respective photosynthetic unit sizes (total BChl/reaction center) of ~51 and 66, when assuming a constant ratio of 32 LH1 bacteriochlorophylls per reaction center as determined previously [29]. From the IRFRR transients obtained with the membrane fractions isolated in the present study (Fig. 2C), the F_V/F_M ratios were determined as 0.7 for chromatophores and 0.43 for developing centers. The functional absorption cross-section of the developing centers at 470 nm, as reflected in the slope of the variable fluorescence transient, was about 25% lower (52 Å^2) than that of chromatophores (71 Å^2). They also displayed about 10 times slower rates of fluorescence relaxation (about 100 vs. 8 ms in chromatophores), indicating only partially active electron transport in the developing centers.

3.3. Measurements on greening batch cultures

The greening of *Rba. sphaeroides* was induced by transferring batch cultures from fully aerobic to semiaerobic conditions through concentrating the cells and lowering the shaking rate [27]. The development of the photosynthetic centers was followed by kinetic fluorescence measurement and biochemical analyses.

The different stages of development showed distinct patterns of IRFRR transients (Fig. 3). In the initial phase of the greening (1 h), the centers exhibited rather low F_V/F_M values and very slow electron transfer turnover (Fig. 4C). These kinetics, recorded in the intact cells, strongly resemble the observed IRFRR transients recorded in the developing center fraction (Fig. 2B), with a partially active electron transport chain [21]. With the progression of the greening, the F_V/F_M ratio increased, reaching a maximum at about 4 h (~0.75). In parallel with the F_V/F_M increase, we observed an accelerated electron transport rate. Finally, there was a slow increase in the size of the light-harvesting complex arrays as documented by the increase in the functional absorption cross-section values (Fig. 4B). These observed σ increases can be attributed to the appearance of the LH2 complex, as demonstrated by an increasing presence of the 800-nm excitation band, which can be quantified by the $\sigma_{795\ nm}$ signal. This signal reached a value of ~105 Å^2 at 24 h, concomitant with an accumulation of enhanced pigment levels as a result of the low oxygen tension maintained in these concentrated cell suspensions (Fig. 4A), which was correlated with a very dense accumulation of vesicular ICM in electron micrographs of thin sections (not shown).

In this experiment, the $OD_{680\ nm}$ of the cell suspension was 2.9 at time 0 and gradually increased to 4.4 after 24 h. The small, ~1.5-fold increase in optical density at 680 nm, typical of the course of these greening experiments (data not

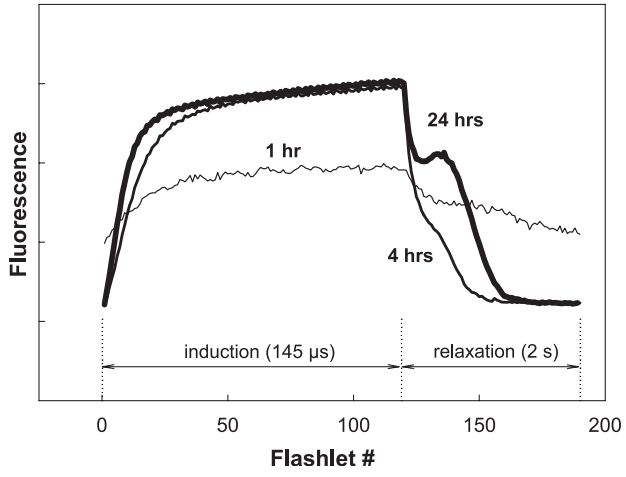

Fig. 3. IRFRR transient elicited upon 470-nm excitation and recorded in different phases of the greening in a low-aeration batch cell suspension. Transient recorded at 1 h (thin solid line) depicts partially active reaction centers; 4-h trace (medium weight solid line) shows fully functional reaction centers with small (mostly LH1) antennae, and 24-h trace (heavy weight solid line) is of fully developed centers with large LH2 antennae and slower electron transfer turnover.

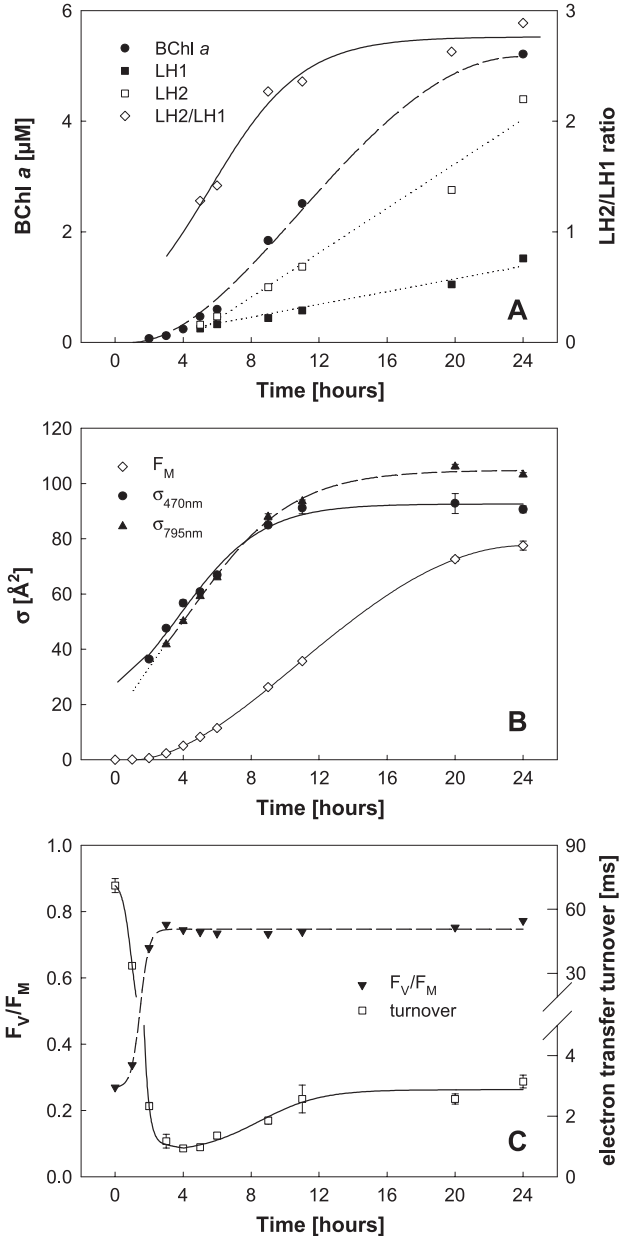

Fig. 4. Analysis of greening in low-aeration batch cell suspensions. (A) Kinetics of ICM induction: molar levels of light-harvesting complexes (LH1, LH2) were determined after deconvolution of absorption spectra as described in Materials and methods. BChl *a* values were calculated from HPLC data. (B) Absolute F_M and functional absorption cross-sections (σ) determined by analysis of IRFRR kinetic transient obtained at 880 nm with whole cell samples after excitation at 470 and 795 nm. (C) F_V/F_M ratios and electron transfer turnover. The displayed values and associated error bars were obtained from three replicate measurements. Parameters are described in the text. In this experiment, the $OD_{680\ nm}$ of the cell suspension was 2.9 at time 0 and gradually increased to 4.4 after 24 h.

shown), indicates that only limited cell division occurred and that these changes largely reflected functional modification in the pigmentation and reaction center functionality in the existing cells. The absorption spectra acquired with whole cells confirmed the differential formation of the LH1 and LH2 antenna complexes [27], in which LH2 becomes the major complex after 4 h, increasing as much as 100-fold over a 24-h duration. In contrast, LH1 levels increased ~25-fold between 2 and 24 h, thereby resulting in a threefold increase in the LH2/LH1 molar ratios over this period reaching a value of ~2.8. Assuming that LH1 contains 32 BChl *a* molecules, we can calculate that at the end of greening the bacterial units contained 122 BChl *a* molecules (32 in LH1 and 90 in LH2). Thus, the increased LH2 levels largely accounted for nearly 100-fold increase in BChl *a* levels over the course of such greening, further explaining the observed increases in both $\sigma_{795\ nm}$ and $\sigma_{470\ nm}$.

3.4. Measurements on greening cultures in a chemostat

Because of the heterogeneity in physiological state inherent to batch cell suspensions, the assembly of photosynthetic units was also examined using continuous cultures grown in a carbon-limited chemostat in the dark. This provided independent control of growth rate and population density; the latter was kept at a constant level by limiting the concentration of organic substrate. The dilution rate and the corresponding growth rate were set to $=1\ day^{-1}$. In this manner, cells were maintained in a defined steady-state growth rate, suitable for physiological studies.

To our surprise, even thoroughly aerated cells in the chemostat contained a small amount of fully functional photosynthetic complexes as seen from the high F_V/F_M values of ~0.8 and rapid electron transfer turnover of ~1 ms (Fig. 5B). The functional cross-section of these complexes was about 28 $Å^2$, indicative of the reaction center–LH1 core complex. Note that the same value was obtained for LH2-deficient mutant M21 (see Table 1). The BChl *a* content in the suspension was about 40 nM and the cellular carbon about 160 mg L^{-1}. This gives a pigment to particulate carbon ratio of 250 nmol BChl *a* g C^{-1}.

After imposing semiaerobic conditions, the growth remained in a steady-state as demonstrated by the essentially constant $OD_{680\ nm}$ values of 0.77 ± 0.05 over the first 24 h (not shown). BChl *a* levels had risen about 40 times over the first 18 h, with a $t_{1/2}$ of ~9 h, up to about 1.2 μM (Fig. 5A), while spheroidenone levels reached a steady state after 24 h (not shown). During the entire period, spheroidenone was maintained as the major carotenoid, whereas spheroidene formed only a minor fraction (<6%). Fig. 5A also presents the results of an analysis of the absorption spectra obtained with whole cells (Fig. 6), which indicated that the LH1–reaction center cores predominated over the first 5 h and were assembled first. This is illustrated by the comparison of the 2-h spectrum with that of cells of the $LH2^-$ M21 mutant (Fig. 6, inset), in which only a small contribution from LH2 is seen in the former, as reflected in the shoulder near 850 nm. Note that although the monomeric BChl band of the reaction center (maximum at 805 nm in

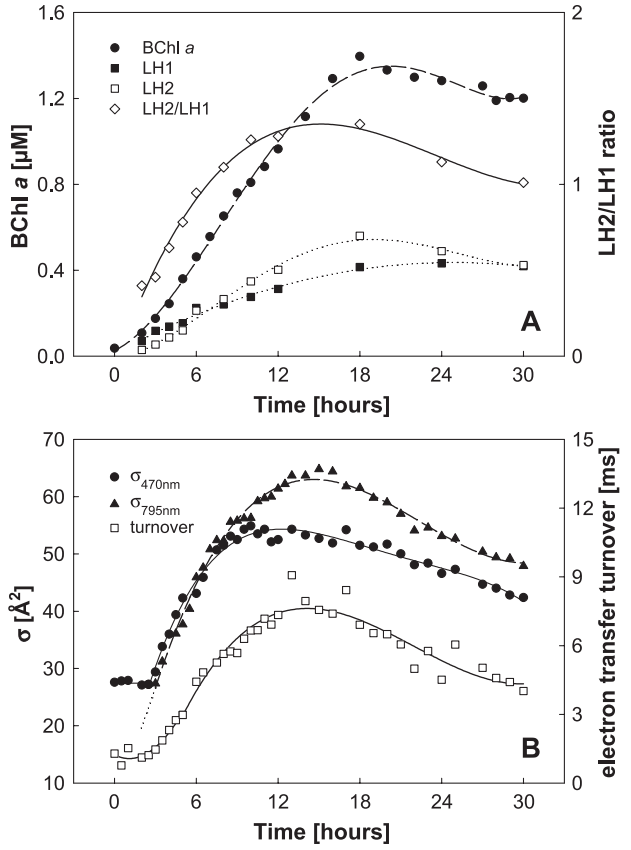

Fig. 5. Analysis of low aeration steady-state cells cultured continuously in a chemostat. Cells were bleached of BChl *a* by pumping air through the culture for 2 days. Then, oxygen tension was lowered to 3% to induce synthesis of both BChl *a* and ICM. (A) Kinetics of ICM induction: molar levels of light-harvesting complexes and BChl *a* values were determined as described in Fig. 4 legend. (B) Functional cross-sections and electron transfer turnover determined by analysis of IRFRR kinetic transients obtained at 880 nm by excitation at 470 and 795 nm. In this experiment F_V/F_M ratios displayed constant values of 0.8.

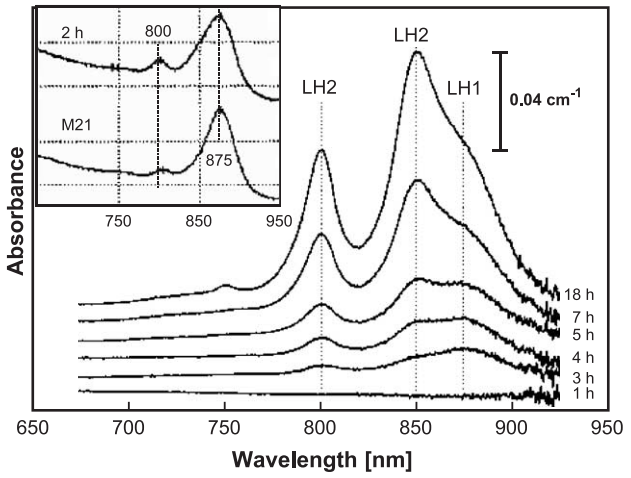

Fig. 6. Near-IR absorption spectra of cells undergoing ICM induction under 3% oxygen in a chemostat. Whole cells were resuspended in 30% bovine serum albumin as described previously [27]. The inset compares the spectra of the 2-h cells and the LH2-deficient mutant M21, which was fully induced at low aeration, and indicates that the 2-h cells are enriched in the LH1–reaction center core complex.

the M21 sample) is obscured by small amounts of B800 and the combined band has a maximum at 802 nm, traces of the 760-nm band of the reaction center are visible in both preparations. These data, together with the $\sigma_{470\ nm}$ values (Fig. 5B), show that assembled LH1–reaction center core particles are present before significant LH2 levels have appeared. It can also be seen in the chemostat culture that LH2 predominated after 6 h, undergoing a nearly 20-fold increase upon reaching a steady-state at 18 h (Fig. 5A), which resulted in a 3.3-fold increase in the LH2/LH1 molar ratio over this period.

The results of an analysis IRFRR fluorescence transients obtained during greening in the chemostat culture are shown in Fig. 5B. The rise in $\sigma_{795\ nm}$ reached steady-state values of ~65 Å^2 at 15–17 h, which essentially mirrored the kinetics of the LH2/LH1 ratio rise shown in Fig. 5A. This is demonstrated in Fig. 7A, which displays a linear relationship between LH2/LH1 ratio and σ_{795nm}. This relationship is expected since both parame-

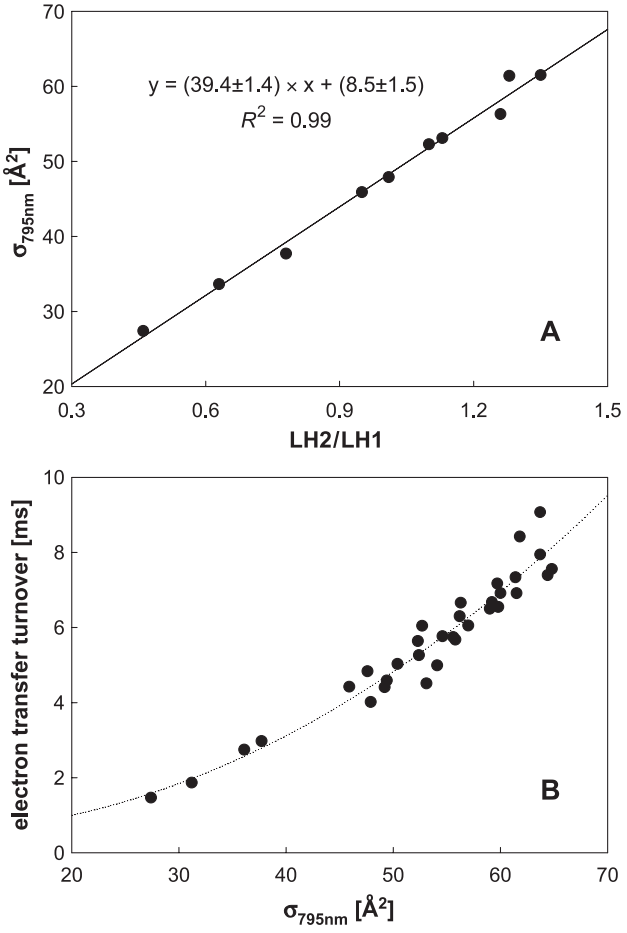

Fig. 7. Panel A: Relationship between LH2/LH1 ratio and functional absorption cross-section at 795 nm. The experimental points were fitted by a linear function. Panel B: Relationship between the size of peripheral light harvesting complex LH2, as determined by functional absorption cross-section at 795 nm, and the electron transfer turnover rate of bacterial reaction center. The experimental points are splined by a quadratic function.

ters reflect the relative size of LH2 antennae per reaction center (size of LH1 per reaction center is constant). In contrast, the $\sigma_{470\ nm}$ rise reached plateau values of ~55 Å^2 earlier, starting at 9.5 h. These final values for σ_{795nm} and $\sigma_{470\ nm}$ were lower than the corresponding values observed in the batch cultures ($\sigma_{795\ nm}$ ~105 Å^2 and the $\sigma_{470\ nm}$ of ~90 Å^2), possibly reflecting the lower pigment levels formed under 3% oxygen. The rates of electron transport were relatively fast (0.8–1.6 ms) after aerobic growth (time=0 h), and during the first 3 h at low aeration (Fig. 5B), but decreased to ~7 ms after about 13 h, similar to the rise in LH2 levels (Figs. 5A and 7B). The F_V/F_M ratio remained fairly constant at ~0.8 during the entire course of the greening (not shown).

Transmission electron micrographs of thin cell sections (Fig. 8) showed that the kinetics of ICM induction in the chemostat culture could be correlated to morphological changes in the intracellular membranes of the inducing cells. At 0 h, the CM is seen mainly in close apposition to the outer membrane, typical of *Rba. sphaeroides* when bleached of photosynthetic pigments [30]. At 2.5 h, the CM had begun to invaginate to from vesicular ICM, while at 6 and 12 h, the cells began to fill up with ICM, reflecting an apparent steady state at 24 h.

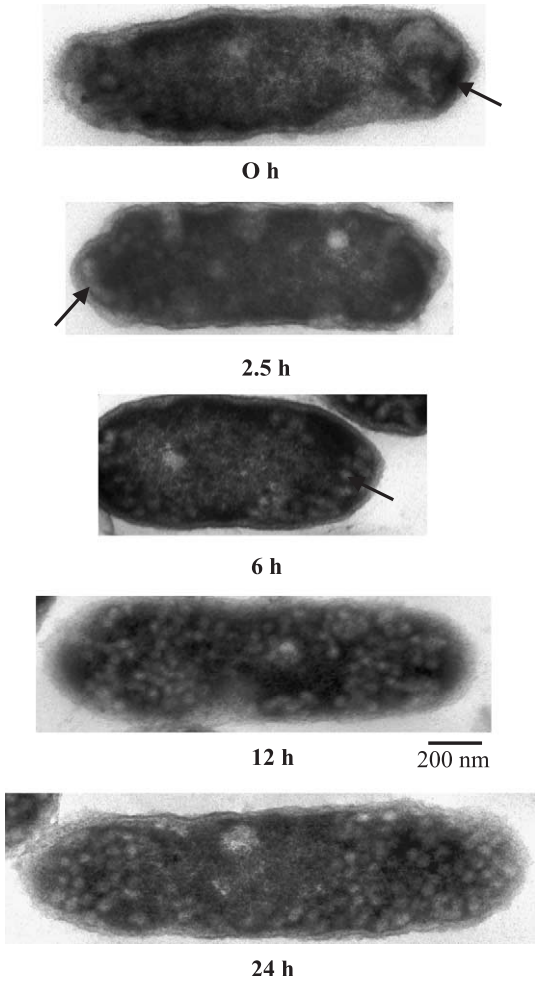

Fig. 8. Electron micrographs of thin sections of cells undergoing ICM induction under 3% oxygen in a chemostat. Fixation, embedding and post-staining procedures are described in Materials and methods. The following are indicated by arrows: 0 h, close apposition between outer membrane and CM; 2.5 h, invagination of CM; 6 h, vesicular ICM.

4. Discussion

4.1. Is the fast repetition rate method applicable for analysis of fluorescence transients in purple non-sulfur photosynthetic bacteria?

The fast repetition rate technique was developed initially for characterization of the physiological status of the photosynthetic apparatus, namely PSII in oxygenic phototrophs [26]. In PSII, variable fluorescence yield principally reflects the redox status of the primary stable electron acceptor Q_A [1]. In photosynthetic bacteria the reports are conflicting. Early reports suggest that fluorescence is governed by the redox status of the primary electron donor P_{870} [2]; however, Q_A might also be the controlling factor [31]. Despite this fact, from a formal point of view, the model used in the IRFRR analysis [26] could be applied independently of whether the fluorescence emission is modulated by the acceptor (PSII) or the donor side (bacterial reaction centers) redox status. The important point is that the initial rapid phase provides single-turnover (single electron transfer) behavior, allowing the basic parameters, such as F_V/F_M ratio, functional absorption cross-section (σ) and connectivity (p), to be obtained. The only difference is that the fluorescence relaxation kinetics might be reflecting the kinetics of P_{870} re-reduction rather than Q_A re-oxidation. For this reason, we have termed the extracted parameter as the electron transfer turnover (τ_{ET}).

There are several lines of evidence that confirm the applicability of the fast repetition rate approach to photosynthetic bacteria. In this study, F_V/F_M ratios in bacteria were found in the range of 0.7–0.8, which roughly agrees with numbers (~0.65) found by Law et al. [31] using terbutryn-inhibited reaction centers. The recorded induction curves frequently displayed close-to-exponential kinetics, suggesting single turnover behavior (sigmoidal kinetics observed in some cases were satisfactorily described by the connectivity model). Also, F_M levels obtained by single turnover flashes were identical to those obtained by multiple turnover pulses of much longer [tens of milliseconds] time scale. The extracted values of functional absorption cross-section ranging from 28 to 100 Å^2 roughly correspond to about 32–120 BChl *a* molecules per bacterial reaction center. For comparison, the green alga *Dunaliella*, possessing about 300 Chl *a* molecules per one PSII, displays functional cross-sections of 200 to 300 Å^2 (Koblizek, unpublished).

4.2. Photosynthetic reaction centers in aerobic cultures of *Rba. sphaeroides*

In the aerobic *Rba. sphaeroides* cultures, small amounts of photosynthetic reaction center activity were demonstrated, despite the low BChl *a* concentration of these cells, which was about two orders of magnitude lower than in their fully pigmented state (Fig. 5A). Such pigment content is comparable with earlier reports [32]. In both batch cultures and the chemostat, these centers displayed identical functional cross-section size of about 28 $Å^2$, corresponding to the reaction center–LH1 core complex characteristic of LH2-deficient mutant M21.

In previous studies, small amounts of the H subunit of the reaction center were demonstrated in immunoblots of aerobic cells [33,34], which together with the reaction center M subunit was thought to exist transiently under these growth conditions [35]. More recently, it has been proposed that the M polypeptide forms the nucleus for assembly of the reaction center complex [36], and it is not surprising that some reaction center activity would be retained in aerobic wild-type cells, since nascent reaction center protein also accompanies the reduced BChl *a* levels. Moreover, a small reaction center primary charge separation has been detected in mutants lacking the H polypeptide [37,38], which retained traces of the reaction center L and M polypeptides in the membrane [37,39,40].

In aerobic batch cultures, we observed partially active reaction center–LH1 core complexes with a low variable fluorescence (F_V/F_M ~0.25) and extremely slow relaxation kinetics (~100 ms), resembling the kinetics of the CM fraction containing the "developing centers" (Fig. 2B). After switching to semiaerobic conditions, these centers were activated (as seen in both F_V/F_M and electron transfer turnover) with a half rise of about 1 h, reaching a fully functional status in 3–4 h. The presence of partially active reaction centers under aerobic conditions is in line with earlier work which showed that although developing centers exhibited EPR signals characteristic of the photo-oxidized reaction center BChl dimer and light-induced reaction center triplet states, signals arising from the Rieske Fe–S center were present at reduced levels [21]. While flash-induced absorption changes indicative of the primary and secondary semiquinone anion acceptor signals were also demonstrated, they were largely unlinked from the bc_1 complex as indicated by the low level of cytochrome b_{561} photoreduction, which, together with the cytochrome c_1/c_2 reactions, occurred at slowed rates. These results suggested that in addition to the insertion of nascent LH1–reaction center core structures into respiratory membrane, the attainment of photosynthetic competence requires proper organization of a fully assembled electron-transport chain.

Interestingly, partially active reaction centers were not observed in the chemostat culture. Instead, rapid electron transfer turnover, as well as a high photochemical yields (F_V/F_M), was detected. To our knowledge, this represents the first observation of a functional reaction center in aerobic *Rba. sphaeroides* cells. The observation of reaction center activity in cells with such low BChl *a* contents [~250 nmol BChl *a* g C^{-1}, or carbon to BChl *a* ratio of 4500

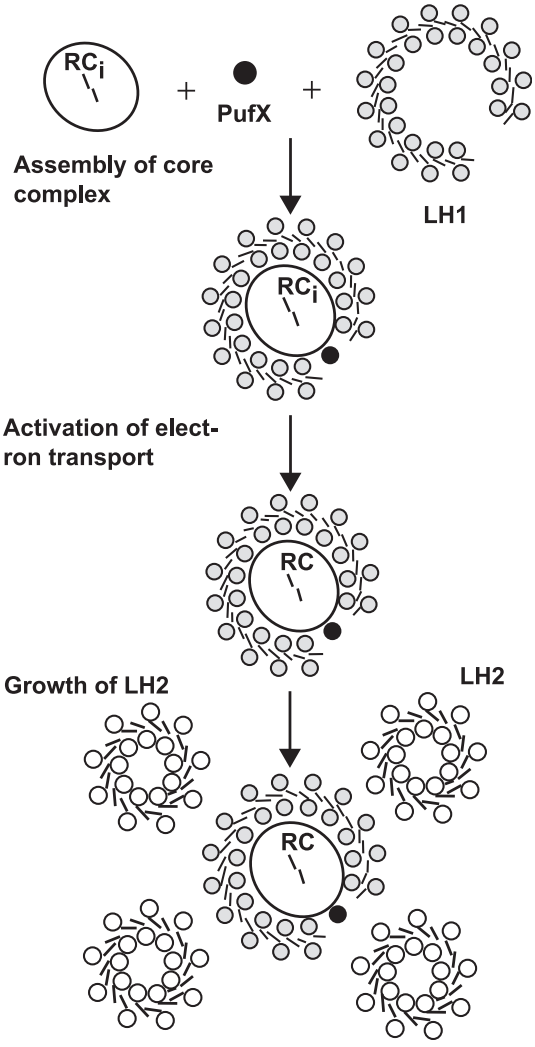

Fig. 9. Structurally based sequential model of bacterial photosynthetic complex assembly. First, core complexes containing an inactive reaction center (RC_i), surrounded by LH1 (outer ring), are assembled in the membrane, along with PufX (black circle). Then, the electron transfer of the assembled cores is activated to give rise to a functional reaction center (RC). Finally, peripheral LH2 (smaller rings) is assembled to provide fully matured photosynthetic complexes. RCs are shown with BChl dimer in center, LH1 as arrays of small stippled circles representing transmembrane α-helices with B875 BChls (end-on view) sandwiched between the inner and outer arrays, and LH2 as array of transmembrane α-helices (open circles) with B850 BChls in between. Complexes are shown in plane of membrane. Studies by Pugh et al. [34] have established that LH1–reaction center cores undergo a time-dependent assembly in which the reaction center appears first, followed by the membrane-organizing PufX core component, prior to encirclement of the reaction center by LH1. Although the cores are depicted here as monomers, they have been shown recently by atomic force microscopy to exist in the ICM of *Rba. sphaeroides* as clusters of dimeric structures [42].

(w/w)] is reminiscent of the reaction center activity of aerobic anoxygenic photoheterotrophic bacteria, which have BChl *a* contents an order of magnitude lower than in phototrophically grown *Rba. sphaeroides* [41].

4.3. Greening of Rba. sphaeroides

After transfer to semiaerobic conditions, an extensive assembly of the peripheral light harvesting complex LH2 was observed in both the chemostat and batch cultures. This process occurred with a half rise of about 6 h and it was completed in about 14 h. Coincident with the growth of LH2 antenna, the electron transfer turnover was slowed. The pattern of changes in the electron turnover could be correlated with the formation of the LH2 antenna (Fig. 7B), rather than with absolute accumulation of BChl *a*, which reached its maximum only later (18 h). This may be related to an imposition of constraints on reaction center activity as the membrane bilayer becomes densely packed with the accumulating LH2 complexes. As expected, the changes of respective functional cross-sections at 470 nm (which monitors carotenoids in both LH1 and LH2) and 795 nm (which exclusively monitors B800 bacteriochlorophylls of LH2) did not occur in parallel (Figs. 4 and 5). This reflects the sequential assembly of the antenna complexes with LH1 appearing first, followed by LH2 which becomes the major complex as the greening proceeds.

The observed biophysical patterns of greening in *Rba. sphaeroides* suggest the following model for photosynthetic complex assembly (Fig. 9). First, proteins of the bacterial reaction center and LH1 are assembled in the CM. Newly assembled reaction center–LH1 complexes have a limited ability to perform charge separation (F_V/F_M values) and are inactive in forward electron transport. This stage corresponds to the CM fraction of "developing centers", isolated by sucrose gradient centrifugation, which showed very similar IRFRR transients. Electron transport is then activated, most likely by the insertion of some additional electron transport component(s), such as the full complement of Rieske iron–sulfur centers [21], possibly reflecting a hierarchy in the global regulatory systems [13,43]. This process does not seem to be completely repressed under aerobic conditions, and after transfer to semiaerobiosis in batch cultures, the activation of the centers occurs rapidly with a half-time of about 1 h. The partially active centers were not seen in the chemostat grown cells, perhaps as a result of differences in physiological state between the two cultures. These activated core complexes are likely to be present in the CM fraction. Finally, reaction center activation is followed by an extensive accumulation of the peripheral antenna complex LH2 [27,44,45] within 18 h after the onset of greening. During this stage, the growth of LH2 antennae stimulates CM invagination producing a fully matured, vesicular ICM.

4.4. Conclusions

This report demonstrates that the IRFRR technique provides a useful and highly sensitive method for study of photosynthetic properties of non-sulfur purple photosynthetic bacteria. This technique permits the determination of photochemical yields, electron transfer turnover and functional absorption cross-sections. Its power was applied in the study of the assembly of intramembrane photosynthetic units in *Rba. sphaeroides*, both in whole cells and in the developing photosynthetic membranes derived from them. In addition, it should prove to be highly valuable in the screening and characterization of genetically engineered mutant strains.

Acknowledgements

This work was supported by Rutgers University through a Postdoctoral Research Fellowship to M.K. and the Charles and Johanna Busch Memorial Fund (R.A.N.). M.K. was also partially supported by the Czech projects GACR 206/03/P079 and MSMT LN00A141. We thank Paul G. Falkowski for the use of laboratory facilities and for reading the manuscript, Valentin Starovoytov for performing the sectioning and transmission electron microscopy, and Marcin K. Kolber for technical assistance.

References

[1] L. Nedbal, M. Koblizek, Chlorophyll fluorescence as a reporter on in vivo electron transport and regulation in plants, in: B. Grimm, R. Porra, W. Ruediger, H. Scheer (Eds.), Advances in Photosynthesis, Biochemistry and Biophysics of Chlorophylls, in: Govindjee (Series Ed.), Kluwer Academic Press, 2004, in press.

[2] K.L. Zankel, D.W. Reed, R.K. Clayton, Fluorescence and photochemical quenching in photosynthetic reaction centers, Proc. Natl. Acad. Sci. U. S. A. 61 (1968) 1243–1249.

[3] C.N. Hunter, R. van Grondelle, N.G. Holmes, O.T.G. Jones, R.A. Niederman, Fluorescence yield properties of a fraction enriched in newly synthesized bacteriochlorophyll *a*–protein complexes from *Rhodopseudomonas sphaeroides*, Photochem. Photobiol. 30 (1979) 313–316.

[4] H.-W. Trissl, Antenna organization in purple bacteria investigated by means of fluorescence induction curves, Photosynth. Res. 47 (1996) 175–185.

[5] K.A. Schmidt, H.-W. Trissl, Combined fluorescence and photovoltage studies on chlorosome containing bacteria: I. Whole cells of *Chloroflexus aurantiacus*, Photosynth. Res. 58 (1998) 43–55.

[6] D.M. Kramer, A. Kanazawa, D. Fleischman, Oxygen dependence of photosynthetic electron transport in a bacteriochlorophyll-containing rhizobium, FEBS Lett. 417 (1997) 275–278.

[7] Z.S. Kolber, C.L. van Dover, R.A. Niederman, P.G. Falkowski, Bacterial photosynthesis in surface waters of the open ocean, Nature 407 (2000) 177–179.

[8] G. Cohen-Bazire, W.R. Sistrom, R.Y. Stanier, Kinetic studies of pigment synthesis by non-sulfur purple bacteria, J. Cell. Comp. Physiol. 49 (1956) 25–68.

[9] J. Takemoto, J. Lascelles, Coupling between bacteriochlorophyll and membrane protein synthesis in *Rhodopseudomonas sphaeroides*, Proc. Natl. Acad. Sci. U. S. A. 70 (1973) 799–803.
[10] M. Sganga, C.E. Bauer, Regulatory factors controlling photosynthetic reaction center and light-harvesting gene expression in *Rhodobacter capsulatus*, Cell 68 (1992) 945–954.
[11] M.K. Phillips-Jones, C.N. Hunter, Cloning and nucleotide sequence of regA, a putative response regulator gene of *Rhodobacter sphaeroides*, FEMS Microbiol. Lett. 116 (1994) 269–276.
[12] J.M. Eraso, S. Kaplan, prrA, a putative response regulator involved in oxygen regulation of photosynthesis gene expression in *Rhodobacter sphaeroides*, J. Bacteriol. 176 (1994) 32–43.
[13] L.R. Swem, S. Elsen, T.H. Bird, D.L. Swem, H.-G. Koch, H. Myllykallio, F. Daldal, C.E. Bauer, The RegB/RegA two-component regulatory system controls synthesis of photosynthesis and respiratory electron transfer components in *Rhodobacter capsulatus*, J. Mol. Biol. 309 (2001) 121–138.
[14] R.J. Penfold, J.M. Pemberton, Sequencing, chromosomal inactivation, and functional expression of ppsR, a gene which represses carotenoid and bacteriochlorophyll synthesis in *Rhodobacter sphaeroides*, J. Bacteriol. 176 (1994) 2869–2876.
[15] S.N. Ponnampalam, C.E. Bauer, DNA binding characteristics of CrtJ. A redox-responding repressor of bacteriochlorophyll, carotenoid, and light harvesting-II gene expression in *Rhodobacter capsulatus*, J. Biol. Chem. 272 (1997) 18391–18396.
[16] S. Masuda, C.E. Bauer, AppA is a blue light photoreceptor that antirepresses photosynthesis gene expression in *Rhodobacter sphaeroides*, Cell 110 (2002) 613–623.
[17] S. Braatsch, M. Gomelsky, S. Kuphal, G. Klug, A single flavoprotein, AppA, integrates both redox and light signals in *Rhodobacter sphaeroides*, Mol. Microbiol. 45 (2002) 827–836.
[18] R.A. Niederman, D.E. Mallon, L.C. Parks, Membranes of *Rhodopseudomonas sphaeroides*. VI. Isolation of a fraction enriched in newly synthesized bacteriochlorophyll *a*–protein complexes, Biochim. Biophys. Acta 555 (1979) 210–220.
[19] P.A. Reilly, R.A. Niederman, Role of apparent membrane growth initiation sites during photosynthetic membrane development in synchronously dividing *Rhodopseudomonas sphaeroides*, J. Bacteriol. 167 (1986) 153–159.
[20] R.A. Niederman, C.N. Hunter, G.S. Inamine, D.E. Mallon, Development of the bacterial photosynthetic apparatus, in: G. Akoyunoglou (Ed.), Photosynthesis, vol. 4, Chloroplasts Development, Balaban, Philadelphia, PA, 1981, pp. 663–674.
[21] J.R. Bowyer, C.N. Hunter, T. Ohnishi, R.A. Niederman, Photosynthetic membrane development in *Rhodopseudomonas sphaeroides*: spectral and kinetic characterization of redox components of light-driven electron flow in apparent photosynthetic membrane growth initiation sites, J. Biol. Chem. 260 (1985) 3295–3304.
[22] C.N. Hunter, J.D. Pennoyer, J.N. Sturgis, D. Farrelly, R.A. Niederman, Oligomerization states and associations of light-harvesting pigment–protein complexes of *Rhodobacter sphaeroides* as analyzed by lithium dodecyl sulfate-polyacrylamide gel electrophoresis, Biochemistry 27 (1988) 3459–3467.
[23] P.J. Kiley, A. Varga, S. Kaplan, A physiological and structural analysis of light harvesting mutants of *Rhodobacter sphaeroides*, J. Bacteriol. 170 (1988) 1103–1115.
[24] J.N. Sturgis, C.N. Hunter, R.A. Niederman, Assembly of intracytoplasmic membranes in *Rhodobacter sphaeroides* mutants lacking light-harvesting and reaction center complexes, in: G. Drews, E.A. Dawes (Eds.), Molecular Biology of Membrane-Bound Complexes in Phototrophic Bacteria, Plenum, New York, 1990, pp. 219–226.
[25] J.N. Sturgis, R.A. Niederman, The effect of different levels of the B800-850 light-harvesting complex on intracytoplasmic membrane development in *Rhodobacter sphaeroides*, Arch. Microbiol. 165 (1996) 235–242.
[26] Z.S. Kolber, O. Prasil, P.G. Falkowski, Measurements of variable chlorophyll fluorescence using fast repetition rate techniques: defining methodology and experimental protocols, Biochim. Biophys. Acta 1367 (1998) 88–106.
[27] R.A. Niederman, D.E. Mallon, J.J. Langan, Membranes of *Rhodopseudomonas sphaeroides*: IV. Assembly of chromatophores in low-aeration cell suspensions, Biochim. Biophys. Acta 440 (1976) 429–447.
[28] J.N. Sturgis, C.N. Hunter, R.A. Niederman, Spectra and extinction coefficients of near-infrared absorption bands in membranes of *Rhodobacter sphaeroides* mutants lacking light-harvesting and reaction center complexes, Photochem. Photobiol. 48 (1988) 243–247.
[29] W.H.J. Westerhuis, J.W. Farchaus, R.A. Niederman, Altered spectral properties of the B875 light-harvesting pigment–protein complex in a *Rhodobacter sphaeroides* mutant lacking *puf*X, Photochem. Photobiol. 58 (1993) 460–463.
[30] G. Cohen-Bazire, Some observations on the organization of the photosynthetic apparatus in purple and green bacteria, in: H. Gest, A. San Pietro, L.P. Vernon (Eds.), Bacterial Photosynthesis, Antioch Press, Yellow Springs, OH, 1963, pp. 89–110.
[31] C.J. Law, R.J. Cogdell, H.-W. Trissl, Antenna organisation in the purple bacterium *Rhodopseudomonas acidophila* studied by fluorescence induction, Photosynth. Res. 52 (1997) 157–165.
[32] A.E. Brown, F.A. Eiserling, J. Lascelles, Bacteriochlorophyll synthesis and ultrastructure of wild-type and mutant strains of *Rhodopseudomonas spheroides*, Plant Physiol. 50 (1972) 743–746.
[33] J. Chory, T.J. Donohue, A.R. Varga, L.A. Staehelin, S. Kaplan, Induction of the photosynthetic membranes of *Rhodopseudomonas sphaeroides*: biochemical and morphological studies, J. Bacteriol. 159 (1984) 540–554.
[34] R.J. Pugh, P. McGlynn, M.R. Jones, C.N. Hunter, The LH1–RC core complex of *Rhodobacter sphaeroides*: interaction between components, time-dependent assembly, and topology of the PufX protein, Biochim. Biophys. Acta 1366 (1998) 301–316.
[35] A.R. Varga, S. Kaplan, Synthesis and stability of reaction center polypeptides and implications for reaction center assembly in *Rhodobacter sphaeroides*, J. Biol. Chem. 268 (1993) 19842–19850.
[36] A. Tehrani, R.C. Prince, J.T. Beatty, Effects of photosynthetic reaction center H protein domain mutations on photosynthetic properties and reaction center assembly in *Rhodobacter sphaeroides*, Biochemistry 42 (2003) 8919–8928.
[37] R.E. Sockett, T.J. Donohue, A.R. Varga, S. Kaplan, Control of photosynthetic membrane assembly in *Rhodobacter sphaeroides* mediated by puhA and flanking sequences, J. Bacteriol. 171 (1989) 436–446.
[38] Y.S. Cheng, C.A. Brantner, A. Tsapin, M.L.P. Collins, Role of the H protein in assembly of the photochemical reaction center and intracytoplasmic membrane in *Rhodospirillum rubrum*, J. Bacteriol. 182 (2000) 1200–1207.
[39] D.K.-H. Wong, W.J. Collins, A. Harmer, T.G. Lilburn, J.T. Beatty, Directed mutagenesis of the *Rhodobacter capsulatus puh*A gene and orf 214: pleiotropic effects on photosynthetic reaction center and light-harvesting 1 complexes, J. Bacteriol. 178 (1996) 2334–2342.
[40] X.-Y. Chen, V. Yurkov, M.L. Paddock, M.Y. Okamura, J.T. Beatty, A puhA gene deletion and plasmid complementation system for facile site directed mutagenesis studies of the reaction center H protein of *Rhodobacter sphaeroides*, Photosynth. Res. 505 (1998) 369–373.
[41] Z.S. Kolber, F.G. Plumley, A.S. Lang, J.T. Beatty, R.E. Blankenship, C.L. Van Dover, C. Vetriani, M. Koblízek, C. Rathgeber, P.G. Falkowski, Contribution of aerobic photoheterotrophic bacteria to the carbon cycle in the ocean, Science 292 (2001) 2492–2495.
[42] S. Bahatyrova, R.N. Frese, C.A. Siebert, J.D. Olsen, K.O. van der Werf, R. van Grondelle, R.A. Niederman, P.A. Bullough, C. Otto, C.N. Hunter, The native architecture of a photosynthetic membrane, Nature 430 (2004) 1058–1062.

[43] J.-I. Oh, S. Kaplan, Redox signaling: globalization of gene expression, EMBO J. 19 (2000) 4237–4247.
[44] A. Schumacher, G. Drews, The formation of bacteriochlorophyll *a* protein complexes of the photosynthetic apparatus of *Rhodopseudomonas capsulata* during early stages of development, Biochim. Biophys. Acta 501 (1978) 183–194.
[45] A.A. Yeliseev, J.M. Eraso, S. Kaplan, Differential carotenoid composition of the B875 and B800-850 photosynthetic antenna complexes in *Rhodobacter sphaeroides* 2.4.1: involvement of spheroidene and spheroidenone in adaptation to changes in light intensity and oxygen availability, J. Bacteriol. 178 (1996) 5877–5883.